VRACK: Measuring Pedal Kinematics During Stationary Bike Cycling

Amir B. Farjadian[1], Qingchao Kong[1], Venkata K. Gade[2], Judith E. Deutsch[2] and Constantinos Mavroidis[1]

[1] Biomedical Mechatronics Laboratory, Department of Mechanical and Industrial Engineering
Northeastern University, 360 Huntington Avenue, Boston MA 02115
Tel: 617-373-4121, Fax: 617-373-2921,
Email: mavro@coe.neu.edu, Webpage: http://www.robots.neu.edu

[2] RIVERS (Research in Virtual Environments & Rehabilitation Sciences) Laboratory
Department of Rehabilitation and Movement Sciences,
University of Medicine and Dentistry of New Jersey, 65 Bergen St., Newark, NJ, 07101-1709 USA
Email: deutsch@umdnj.edu; Webpage: http://shrp.umdnj.edu/rivers/

Ankle impairment and lower limb asymmetries in strength and coordination are common symptoms for individuals with selected musculoskeletal and neurological impairments. The virtual reality augmented cycling kit (VRACK) was designed as a compact mechatronics system for lower limb and mobility rehabilitation. The system measures interaction forces and cardiac activity during cycling in a virtual environment. The kinematics measurement was added to the system. Due to the constrained problem definition, the combination of inertial measurement unit (IMU) and Kalman filtering was recruited to compute the optimal pedal angular displacement during dynamic cycling exercise. Using a novel benchmarking method the accuracy of IMU-based kinematics measurement was evaluated. Relatively accurate angular measurements were achieved. The enhanced VRACK system can serve as a rehabilitation device to monitor biomechanical and physiological variables during cycling on a stationary bike.

***Key Words*—Lower limb rehabilitation, Kinematics measurement, Inertial measurement unit, Kalman Filter.**

I. Introduction

Ankle injuries are common disorders that can occur due to overuse, trauma, and neural degenerations. Central and peripheral damage to nervous system can result in loss of coordination and range of movement (ROM) at the ankle joint. Ankle sprains represent 2.15 per 1000 person-years in the United States [1], with about 50% of occurrence during athletic exercise. In patients with neurological conditions such as stroke, ankle incoordination and weakness are common impairments that may interfere with activities of daily living (ADL) such as walking, running, and postural stability.

Ankle joint is the distal effector in cycling. Cycle ergometry has been applied particularly for ankle rehabilitation and more generally to lower extremity (LE) in varied populations and at different phases of recovery. Cycling has been included in the rehabilitation of individuals in the sub-acute stage of high ankle sprains [2] with the goal of normalizing joint mobility. It was also recruited in the rehabilitation of individuals with Duchene MD [3] focusing on the LE endurance. Although measuring the ankle ROM may have not been the primary goal, cycling has been prescribed as a component of intensive rehabilitation exercise to promote LE endurance and improve mobility post-stroke [4-6]. Most recently a trial has been proposed to establish efficacy of cycling ergometry as a form of repetitive functional training necessary for people in the early days post-stroke [7].

The partially documented benefits of cycling spans improved aerobic fitness [8-9], increased muscle strength [10-12] and even transfer to other activities such as walking [9, 11]. Cycling has been performed in isolation, or in combination with electrical stimulation [9-11], and with augmented virtual reality (VR) environment [13]. With the purpose of coupling the assets of VR interface [14] with the benefits of cycling, the virtual reality augmented cycling kit (VRACK) was designed and implemented [15-16].

The VRACK is a novel mechatronics system designed as a rehabilitation device to monitor biomechanical and physiological variables during cycling on a stationary bike. In the first version of this system the interaction forces of pedals and handlebars [15-16]; as well as the heart rate monitoring capabilities [17] were addressed. These inputs were transmitted into the VR environment to drive the behavior of the cycling avatar, and also used to record the cyclist's performance.

In the current iteration, the role of ankle kinematics during cycling was considered. Ankle joint's kinematics can be used to identify mechanical efficiency, which has been associated with a more plantar-flexed ankle through the top and downstroke of the pedal cycle and more dorsi-flexed during the upstroke. Moreover the coupling of kinetic and kinematic data from the pedals can serve a surrogate measure of the rider's underlying motor control. However due to our constrained problem definition, measuring the pedal kinematics was not a straightforward task.

An Inertial Measurement Unit (IMU) is a combination of accelerometers and gyroscopes that is widely used in

978-1-4673-6024-1/13/$31.00 ©2013 IEEE

navigation problems to measure velocity and orientation [18]. Sensitive to gravity, these micromechanical systems (MEMS) have been integrated into monitoring systems to record human movements outside laboratory environments [19]. Other applications span monitoring ADL and level of activity [20], human motor control and stability [21], load estimation and functional electrical stimulation [22]. Owing to our specific problem definition of having a standalone cycling kit independent from the stationary bike body, IMUs were selected for the VRACK system to measure the pedal kinematics. Both pedals were equipped with IMUs to collect acceleration and gyro and compute pedal angular displacements with respect to the external observer.

The common challenge in using IMU sensors is the excessive amount of noise in the acquired signals that leads to inaccurate measurements. This problem is caused by the highly sensitive internal MEMS structure, and also the dependency upon variety of environmental conditions such as temperature, gravity or fluctuations in the supply voltage [23-4]. The accuracy of the acquired signal can be increased by using advanced signal processing methods. There is a body of research on using IMU with Kalman filter in various fields including navigation of autonomous vehicles, camera calibration, and rehabilitation [25-8]. But most of these applications have low or negligible acceleration with respect to gravity. The application of IMU was not recommended for problems with relatively comparable instantaneous acceleration amplitude with respect to gravity, such as cycling.

In this paper, the brief description of the VRACK system is presented. The integration of IMU in the smart pedal structure, to measure the pedal acceleration and gyro with respect to the external reference, is explained. The application of Kalman filter to process the noisy IMU data channels and compute the pedal angle is discussed. The benchmarking setup to assess the accuracy of the final pedal kinematics during cycling is presented.

II. System Overview

The complete building components of the virtual reality augmented cycling kit (VRACK) are presented in Figure 1. The primary engineering problem was to build an independent, compact cycling kit to be assembled on a typical stationary bike with the purpose of assessing human biomechanical interaction with this popular exercise equipment. The system was engineered with two sensorized pedals (B), two handlebars with hydraulic pressure sensors (A) and a heart rate monitor (D). Two separate visual media were considered for the patient and the therapist. Virtual reality (F) was used as an interface with the human subject and more elaborate measures were integrated into the practitioner interface for monitoring purposes (E).

Two smart pedal modules, shown in Figure 2, are installed on the stationary bike that host force and angle measurement transducers. The applied force to the pedal raceway is transferred to a load cell (LC302-500, Omega Engineering), using a force-transition mechanism, so as to measure the interaction forces between the subject's foot and the pedal. This force sensing mechanism is calibrated to measure -20 lbs. (≈ -90 N) of tensile force to +100 lbs. (≈ 450 N) of compression force. The kinematics measurement capability of the smart pedals is described in the next section.

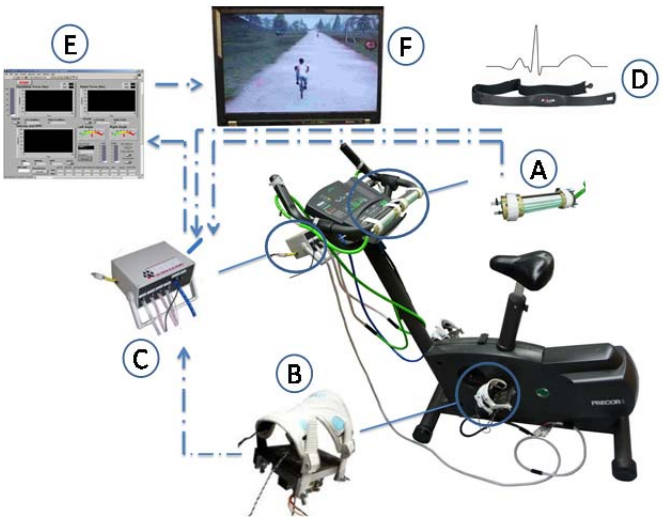

Fig. 1. VRACK system complete overview; A: Handlebar module; B: Smart pedal; C: Power supply, preamplifier and the data acquisition board; D: Heart rate monitor, E: Practitioner interface; F: Virtual reality environment.

Two sensorized handlebars with hydraulic pressure sensors (PX35, Omega Engineering) are installed around the mechanical handlebars of the stationary bike. Subjects grasp the sensorized handlebars, and apply force, to control the bike balance during ongoing simulated cycling in the virtual reality environment.

The wireless heart rate monitor (RE07L, Polar Electro Inc.) is strapped around the patient's chest to measure heart rate during cycling exercise. This physiological variable is used by the practitioner, to set the training intensity by adjusting the speed of the pacer in the VR game.

The biomechanical and physiological variables are collected using the data acquisition board (NI-USB 6216) and transferred to the self-developed code (LabVIEW 8.2, National Instruments Corp.). The acquired data is demonstrated in real-time in practitioner interface; is recorded in a text file for post processing and drives the virtual reality game.

With the purpose of entertainment and more engagement for the patient, the virtual reality game showing a cycling avatar is displayed. The avatar speed is controlled by the pedaling speed. His direction and postural balance are controlled, respectively, by the measured forces at the handlebars and the force balance among the left\right pedals. The vibration feedback, installed on the pedal foot binding, is triggered when riding off the road into the surrounding grassy verge area.

The practitioner interface is a more technical medium for the purpose of activity monitoring during exercise in real-time. The practitioner is able to follow the instantaneous applied forces to both pedals and handlebars, monitor the pedaling speed and heart rate status.

III. METHODS

During cycling, the principal components of ankle joint movements are dorsiflexion and plantarflexion. The ergonomic foot bindings (Flow Snowboarding, CA, USA) were used to strap and secure the patient's feet to the pedal raceway. This arrangement was employed to transfer the slightest changes in the ankle joint to the pedals.

In a typical bike structure, the pedal body is fastened to the crank arm with the pedal shaft. A set of ball bearings are between the pedal body and the pedal shaft. Consequently the pedal shaft is fixed relative to the crank arm. The pedal rotates freely relative to the pedal shaft, and the crank arm. Cycling as defined by rotating the crank arm, relative to the external reference, is accompanied by the pedal rotation with respect to the crank.

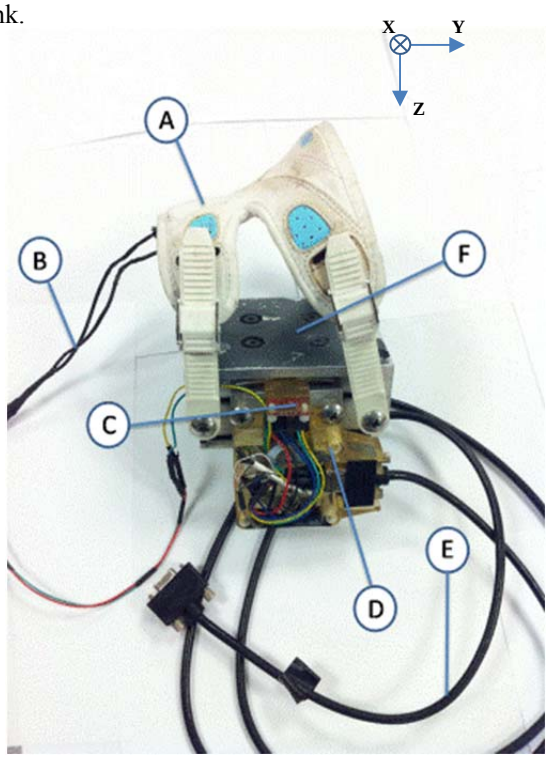

Fig. 2. The smart pedal components. A: Ergonomic foot bindings; B: Detachable vibration element; C: Inertial measurement unit; D: Electronics safety enclosure; E: High-flexibility double shielded cable; F: Pedal raceway.

Due to this intrinsic complexity in the pedal-bike force transmission structure, measuring the pedal angle with respect to the external reference is not a straightforward task. This issue was more stressed in our compact design problem, so as to have an independent module from the stationary bike. Accordingly the combination of IMU sensor with advanced post-processing Kalman filtering was used for this application.

A. Hardware

A 3D accelerometer unit can be used as an inclinometer to measure the angle of the pedal with respect to the vector of gravity [16-20]. This method was mostly practiced in the absence of externally applied acceleration or if the magnitude of the dynamic acceleration is negligible with respect to the gravity [17]. Gyroscope can also be used, as an additional source of the same measure, to be fused with the accelerometer data and provide a more accurate angle measurement.

The 5-degrees of freedom IMU (SEN-09268, Sparkfun Electronics) was used for the purpose of measuring the pedal angle with respect to the external reference. The electronic circuit board is composed of a two-axis vibrating beam gyroscope (IDG500) and a three-axis piezo-resistive accelerometer (ADXL335), on a 20*23 mm^2 printed circuit board with less than 5 g weight. This sensitive MEMS structure provides the possibility of collecting the angular velocity in roll and pitch orientation in addition to the acceleration along X, Y and Z axes, as shown in Figure 2.

As shown in Figure 2, the IMU was placed in a face-down position parallel to the pedal raceway. Considering this placement with respect to gravity, the pedal angle can be computed from the gyroscope, by taking the integral of the roll (ω) component, as well as the angle between Y and Z components of the accelerometer:

$$\theta_{acc} = \arctan\left(\frac{a_y}{a_z}\right) \quad (1)$$

Due to the inherent large amount of noise in the IMU data, the computed angular displacement during human cycling was very noisy and henceforth unreliable. This problem was more significant in the dynamic cycling activity, which has comparable acceleration to gravity. Kalman filtering was recruited as a post-processing step to improve the accuracy of the final measurements.

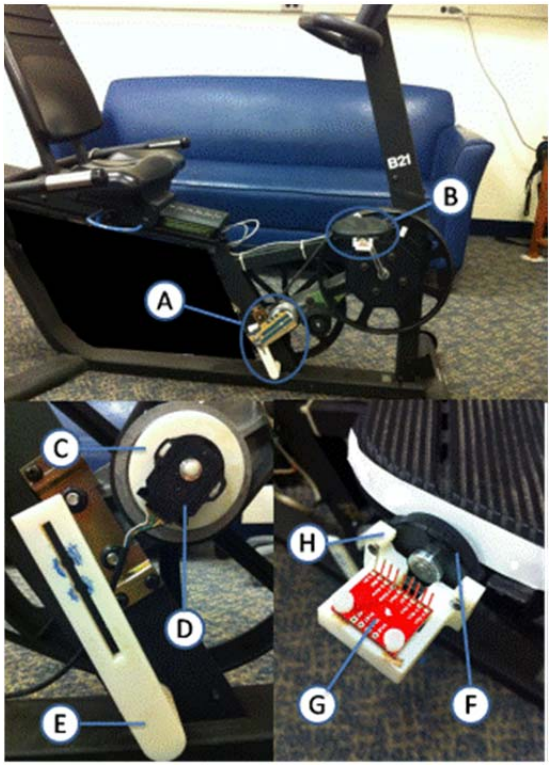

Fig. 3. IMU benchmarking setup. A: Encoder circuit on the grooved pulley; B: Encoder and IMU on the test-pedal; C, E and H: Mechanical adaptors made by 3D printer; D: Optical encoder on the grooved pulley; F: Optical encoder on the test-pedal; G: Face-down IMU PCB.

B. Benchmarking

The Kalman filter algorithm was used to fuse the acceleration and angular velocity and compute the angular displacement. This method is explained in the appendix.

The rotary encoder is a sensor that converts the motion of the central axle to a measurable voltage. The axle or the shaft rotates relative to the encoder body. In order to assess the accuracy of the final pedal kinematics measurement, IMUs were fabricated, in a similar orientation, in a separate test-pedal structure along with an encoder, as a direct reference from angular displacement. The benchmarking circuit was installed on the stationary recumbent bike (Cybex 700R), as shown in Figure 3. The benchmarking setup consisted of two relative optical encoders (RCML 15, RENCO). One was fabricated with the IMU to the test-pedal, and the second encoder was fabricated to the grooved (rear) pulley of the bike.

Two encoders were installed on the grooved pulley and the test-pedal with the efficient fabrication and housing structures so as to collect angular displacement. The encoder circuit A was mounted on the grooved pulley of the stationary bike to measure the crank angle with respect to the global reference. The encoder circuit B was mounted on the test-pedal shaft to measure the pedal angle with respect to the crank. The subtraction of the two measures, by considering the pulley diameters, is the pedal angular displacement with respect to the global reference.

Installation of encoders on the pedal shaft and grooved pulley required manufacturing and fabrication of mechanical motion transmission structures. The mechanical components were designed in 3D computer-aided design (CAD) software (SolidWorks 2012) and manufactured using rapid prototyping by 3D printer (EDEN 333, Stratasys Ltd.).

The error in pedal angle measurement was defined as the difference between the calculated angle from the encoders and the outcome from the IMU and the Kalman filter:

$$\sigma = \theta_{encoders} - \theta_{KF-IMU} \quad (2)$$

The performance index for the method was considered as the root mean squared (RMS) value of the instantaneous error:

$$RMS(\sigma) = \sqrt{\int_{t_1}^{t_2} \sigma^2(t)dt} \quad (3)$$

The data was collected in LabVIEW at 500 Hz sampling rate and transferred to MATLAB (R2012b, Natick, USA) for post-processing. The nominal pulley ratio was calculated (r = 13"/3"), this value was experimentally measured as 0.23635. All raw data was filtered by a 2nd order Butterworth low-pass filter at 50 Hz cut-off frequency prior to post- processing.

IV. Results

In the first step, the left IMU was fabricated on the left test-pedal. A single male healthy subject was recruited to perform the cycling exercise. He was positioned on the sixth grade of the seat shuttle on the recumbent stationary bike, with his knee joint fairly extended. He was instructed to cycle at his comfortable speed. Ten trials, each 45 sec, were collected.

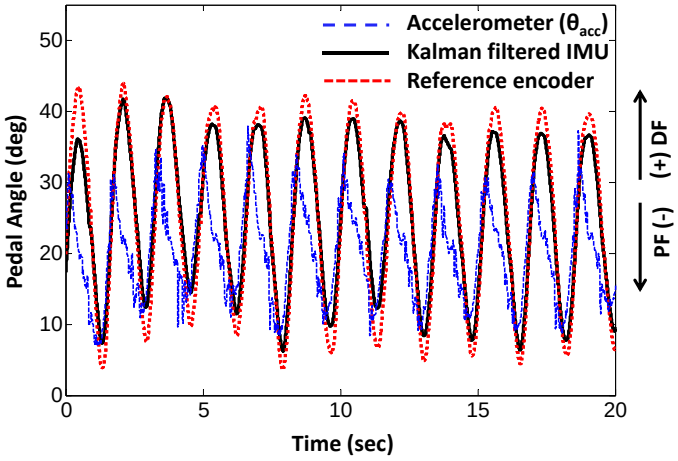

Fig. 4. The angular displacement of the left pedal during cycling; the computed angle from accelerometer raw data in Equation 1 (dashed line), the filtered IMU (solid line), reference profile (dotted line). Dorsiflexion is in positive direction and Plantarflexion is toward negative direction. Positive range of data is due to the subject extended leg posture on the bike.

The IMU was calibrated according to the manufacturer instructions. The Kalman filter was used to fuse the gyro and acceleration data and compute the optimal estimate for the pedal angle. Accordingly the roll (ω) from the gyroscope was considered as the input vector and the θ_{acc} from the accelerometer, as in Eq. 1, was considered as the measured noisy output. The state space equations were framed as:

$$\hat{\theta}'_k = \hat{\theta}_{k-1} + \omega dt \quad (4)$$

$$y_k = \theta_{acc} \quad (5)$$

Accordingly the state space parameters were considered as, A = 1, $B = dt$ (= 0.002 sec), and C = 1 and the initial condition was set to zero. The measurement noise (v) and process noise (w) were estimated using the variance of the accelerometer and gyroscope respectively ($v = \theta_{acc}$, $w = \omega dt$). These values were computed while the pedal, and hence the IMU, was left stationary on the bike. The probability distribution of these random variables was compared to the presumed Gaussian distribution. The corresponding variances (Q, R) were estimated and inserted into the Kalman filter algorithm, so as to achieve the most accurate results. The initial conditions were set to zero. The ultimate angle displacement from the encoder and the Kalman filter were filtered by the 2nd order Butterworth high-pass filter at 0.01 Hz cut-off frequency to remove constant or drift components.

Left pedal's angular displacement data from different sources during cycling is demonstrated in Figure 4. Due to the Kalman filter convergence time in the beginning of the trial, the RMS value was computed after t_1 = 5 sec. Accordingly the computed RMS for the above trial was 2.70 deg and for the whole exercised 10 trials in this experiment was 2.61 ± 0.10 deg.

The same procedure was conducted for the right test-pedal. The computed RMS value for the corresponding 10 trials of the right pedal was 2.77 ± 0.14 deg.

V. Discussion and Conclusion

The basic problem definition was to design a set of smart pedals so as to measure the lower extremity kinetics and kinematics during cycling task. We could not install any sensor on the bike body as our compact design problem was restricted to two instrumented pedals. This paper was focused on the pedal kinematics measurement.

The application of IMU to measure angular displacement, post-processed by Kalman filter, was presented. The novel benchmarking method by optical encoders provided an accurate reference for the computed angle. The Kalman filter was used to compute the statistically optimal measure of a pedal angle, from two noisy measurements. Derivatives of angular displacement, from two separate sources (accelerometer and gyroscope), were fused to compute a more accurate estimate. In spite of the large acceleration amplitude during the cycling task, the computed accuracy was comparable to the reported values in the literature [17].

While cycling at lower speeds resulted in a better accuracy, filter coefficients (Q, R) needed minimal tuning to provide similar accuracy at higher pedaling speeds. The transient convergence time of the Kalman filter, in the first 5 sec of the trial, is rooted in the filter adaptation process. This transient time can be significantly reduced by utilizing the priori knowledge from the previous trials. The positive range of angular displacement, as in Figure 4, is due to the subject extended leg posture on the bike. The effect of gyroscope offset was not significant in this application. This might be due to the short time period of the collected trials.

The VRACK is a compact mechatronics system to measure biomechanical and physiological data during cycling exercise while immersing them in a virtual reality simulation. The system provides visual, auditory and haptic feedback to the subjects. The therapist can customize the exercise in real-time and quantitatively monitor the intervention during the ongoing exercise. The collection of kinetics with kinematic measurements can serve as a unique platform for the physical therapy of ankle injuries and asymmetries in lower extremities.

In the future work, implementation of real-time Kalman filter will be considered into the practitioner interface. Due to the limited achievable accuracy in the IMU measurements, the application of encoders with a new pedal design will be reconsidered. This modification will also enable us to compute the crank angle. By considering the relatively fixed position of the individuals hip joint (and center of crank), anthropometric data can be collected to estimate the leg segment orientation on the pedal. Accordingly the fairly accurate ankle kinematics can be computed, due to this reform.

The force transmission mechanism may also be replaced, with a lower friction structure, to improve the accuracy of force measurements during dynamic cycling task. The high fidelity of the ankle kinematics measures coupled with the kinetic variables will provide a biological variable, measure of stiffness, to aid in rehabilitation of ankle impairments and lower limb asymmetries. The system has to potential to deepen our understanding from human motor control of lower extremities and movement disorders.

Appendix (Kalman filter)

In his seminal paper Kalman presented a state-based filter that has been used in IMU applications [29]. The discrete Kalman filter (DKF) uses a state-space recursive model that is updated based on two physical sensor readings, with dissimilar uncertainties. The early version of the Kalman filter was developed for the state ($x \in R^n$) estimation problem of the following stochastic linear system:

$$x_{k+1} = Ax_k + Bu_k + w_k \quad (6)$$
$$y_k = Cx_k + v_k \quad (7)$$

Where $u \in R^p$ is the input vector; $y \in R^m$ is measured output; $A_{n\times n}$ is the state matrix; $B_{n\times p}$ is the input matrix; $C_{m\times n}$ is the output matrix.

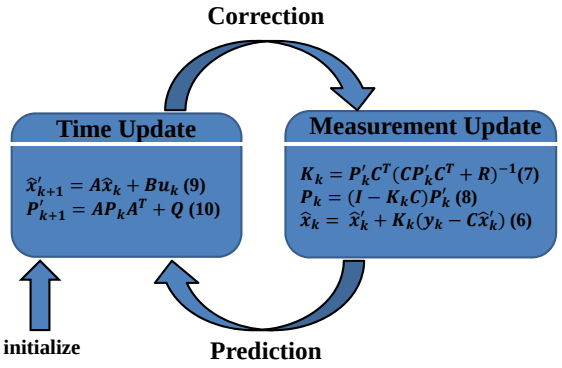

Fig. 5. The Kalman filter algorithm.

The random variables v, w represent the measurement and the process noise respectively. They are assumed to independent with white Gaussian distribution, with zero mean and constant covariance matrices R, Q.

The overall objective is to find the optimal estimate $\hat{x}_k$ of the internal state vector x_k. The error cost function is termed as:

$$e_k = x_k - \hat{x}_k \quad (8)$$
$$P_k = E[e_k e_k^T] \quad (9)$$

P_k is the mean squared error to be minimized. Assuming the prior estimate of $\hat{x}_k$ is called $\hat{x}'_k$, the update equation for the new estimate is given by:

$$\hat{x}_k = \hat{x}'_k + K_k(y_k - C\hat{x}'_k) \quad (10)$$

Where K_k is the Kalman gain; and the term in the right parentheses is called the innovation or measurement residual. By replacing Eq. 10 and Eq. 8 into Eq. 9 and looking for the minimum in the formulated quadratic function, the optimal Kalman gain is computed as:

$$K_k = P'_kC^T(CP'_kC^T + R)^{-1} \quad (11)$$
$$P_k = (I - K_kC)P'_k \quad (12)$$

Where P'_k is the prior estimate of P_k. Equation 12 is the update equation for the error covariance matrix with optimal gain. The last three Equations 10-12 can be used to project an

estimate of the priori state variable $\hat{x}'_{k+1}$ and the covariance matrix P'_{k+1} as:

$$\hat{x}'_{k+1} = A\hat{x}_k + Bu_k \quad (13)$$

$$P'_{k+1} = AP_kA^T + Q \quad (14)$$

The procedural algorithm of the Kalman filter is presented in Figure 5. The generic version of the DKF has five main equations, two in the time update or prediction (Eqs. 13-14) and three in the measurement update or correction (Eqs. 10-12).

The ultimate goal of the filtering process is to find the best estimate of the internal state x_k. The mathematical model of the physical system, i.e. A, B, C matrices in Eqs. 6-7, are assumed to be known as the priori knowledge. Also the input and output vectors are physically measurable. At every time step, the next a priori state estimate is computed by using the preceding optimal state estimate and the known physical model. This step is called prediction as it offers the first guess for the internal state vector. In the correction step, the predicted priori state estimate will be revised by the physically measured output vector.

ACKNOWLEDGEMENTS

This work was supported by the National Institutes of Health (NIH) with the grant R41 HD54261 (PI Judith Deutsch).

REFERENCES

[1] B. R. Waterman, B. D. Owens, S. Davey, M. A. Zacchilli, and P. J. Belmont Jr, "The epidemiology of ankle sprains in the United States," J Bone Joint Surg Am, vol. 92, no. 13, pp. 2279–2284, Oct. 2010.

[2] G. N. Williams and E. J. Allen, "Rehabilitation of Syndesmotic (High) Ankle Sprains," Sports Health: A Multidisciplinary Approach, vol. 2, no. 6, pp. 460–470, Nov. 2010.

[3] M. Jansen, I. J. de Groot, N. van Alfen, and A. C. Geurts, "Physical training in boys with Duchenne Muscular Dystrophy: the protocol of the No Use is Disuse study," BMC Pediatrics, vol. 10, no. 1, p. 55, Aug. 2010.

[4] T. Fujiwara, M. Liu, and N. Chino, "Effect of pedaling exercise on the hemiplegic lower limb," Am J Phys Med Rehabil, vol. 82, no. 5, pp. 357–363, May 2003.

[5] A. Tang, K. M. Sibley, S. G. Thomas, M. T. Bayley, D. Richardson, W. E. McIlroy, and D. Brooks, "Effects of an Aerobic Exercise Program on Aerobic Capacity, Spatiotemporal Gait Parameters, and Functional Capacity in Subacute Stroke," Neurorehabil Neural Repair, vol. 23, no. 4, pp. 398–406, May 2009.

[6] M. Katz-Leurer, I. Sender, O. Keren, and Z. Dvir, "The influence of early cycling training on balance in stroke patients at the subacute stage. Results of a preliminary trial," Clin Rehabil, vol. 20, no. 5, pp. 398–405, May 2006.

[7] N. J. Hancock, L. Shepstone, P. Rowe, P. K. Myint, and V. Pomeroy, "Clinical efficacy and prognostic indicators for lower limb pedalling exercise early after stroke: study protocol for a pilot randomised controlled trial," Trials, vol. 12, p. 68, 2011.

[8] B. Eder, P. Hofmann, S. P. von Duvillard, D. Brandt, J.-P. Schmid, R. Pokan, and M. Wonisch, "Early 4-week cardiac rehabilitation exercise training in elderly patients after heart surgery," J Cardiopulm Rehabil Prev, vol. 30, no. 2, pp. 85–92, Apr. 2010.

[9] T. W. Janssen, J. M. Beltman, P. Elich, P. A. Koppe, H. Konijnenbelt, A. de Haan, and K. H. Gerrits, "Effects of electric stimulation-assisted cycling training in people with chronic stroke," Arch Phys Med Rehabil, vol. 89, no. 3, pp. 463–469, Mar. 2008.

[10] E. Ambrosini, S. Ferrante, A. Pedrocchi, G. Ferrigno, and F. Molteni, "Cycling Induced by Electrical Stimulation Improves Motor Recovery in Postacute Hemiparetic Patients A Randomized Controlled Trial," Stroke, vol. 42, no. 4, pp. 1068–1073, Apr. 2011.

[11] M. J. Lee, S. L. Kilbreath, M. F. Singh, B. Zeman, S. R. Lord, J. Raymond, and G. M. Davis, "Comparison of effect of aerobic cycle training and progressive resistance training on walking ability after stroke: a randomized sham exercise-controlled study," J Am Geriatr Soc, vol. 56, no. 6, pp. 976–985, Jun. 2008.

[12] S. Ferrante, E. Ambrosini, P. Ravelli, E. Guanziroli, F. Molteni, G. Ferrigno, and A. Pedrocchi, "A biofeedback cycling training to improve locomotion: a case series study based on gait pattern classification of 153 chronic stroke patients," Journal of NeuroEngineering and Rehabilitation, vol. 8, no. 1, p. 47, Aug. 2011.

[13] C. H. Chen, M.-C. Jeng, C.-P. Fung, J.-L. Doong, and T.-Y. Chuang, "Psychological benefits of virtual reality for patients in rehabilitation therapy," J Sport Rehabil, vol. 18, no. 2, pp. 258–268, May 2009.

[14] A. Rizzo and G. J. Kim, "A SWOT Analysis of the Field of Virtual Reality Rehabilitation and Therapy," Presence: Teleoperators and Virtual Environments, vol. 14, no. 2, pp. 119–146, Apr. 2005.

[15] R. Ranky, M. Sivak, J. Lewis, A. V. Gade, J. E. Deutsch and C. Mavriodis (In Review) Modular mechatronic system for stationary bicycles interfaced with virtual environment for rehabilitation of patients with movement assymmetry, Journal of Neural Rehabilitation.

[16] R. Ranky, M. Sivak, J. Lewis, V. Gade, J. E. Deutsch, and C. Mavroidis, "VRACK – virtual reality augmented cycling kit: Design and validation," in Proceedings of the 2010 IEEE Virtual Reality Conference, Washington, DC, USA, 2010, pp. 135–138.

[17] J. E. Deutsch, M. J. Myslinski, R. Ranky, M. Sivak, C. Mavroidis, J. A. Lewis, Metabolic response to virtual reality augmented cycling training, Proceedings of the ICDVRAT 2012 Meeting, Laval, France pp. 97-103.

[18] H. J. Luinge and P. P. H. Veltink, "Measuring orientation of human body segments using miniature gyroscopes and accelerometers," Med. Biol. Eng. Comput., vol. 43, no. 2, pp. 273–282, Apr. 2005.

[19] C. Strohrmann, H. Harms, G. Tröster, S. Hensler, and R. Müller, "Out of the lab and into the woods: kinematic analysis in running using wearable sensors," in Proceedings of the 13th international conference on Ubiquitous computing, New York, NY, USA, 2011, pp. 119–122.

[20] C. V. C. Bouten, K. T. M. Koekkoek, M. Verduin, R. Kodde, and J. D. Janssen, "A triaxial accelerometer and portable data processing unit for the assessment of daily physical activity," IEEE Transactions on Biomedical Engineering, vol. 44, no. 3, pp. 136 –147, Mar. 1997.

[21] B. Najafi, K. Aminian, F. Loew, Y. Blanc, and P. A. Robert, "Measurement of stand-sit and sit-stand transitions using a miniature gyroscope and its application in fall risk evaluation in the elderly," IEEE Transactions on Biomedical Engineering, vol. 49, no. 8, pp. 843 –851, Aug. 2002.

[22] H. J. Luinge, P. H. Veltink, and C. T. M. Baten, "Ambulatory measurement of arm orientation," Journal of Biomechanics, vol. 40, no. 1, pp. 78–85, 2007.

[23] J. R. Vig and Y. Kim, "Noise in microelectromechanical system resonators," IEEE Transactions on Ultrasonics, Ferroelectrics and Frequency Control, vol. 46, no. 6, pp. 1558 –1565, Nov. 1999.

[24] S. D. Senturia, "Microsystem Design," Kluwer Academic Publishers, 2001.

[25] F. M. Mirzaei and S. I. Roumeliotis, "A Kalman Filter-Based Algorithm for IMU-Camera Calibration: Observability Analysis and Performance Evaluation," IEEE Transactions on Robotics, vol. 24, no. 5, pp. 1143 –1156, Oct. 2008.

[26] S. Sukkarieh, E. M. Nebot, and H. F. Durrant-Whyte, "A high integrity IMU/GPS navigation loop for autonomous land vehicle applications," IEEE Transactions on Robotics and Automation, vol. 15, no. 3, pp. 572 –578, Jun. 1999.

[27] R. Zhu and Z. Zhou, "A real-time articulated human motion tracking using tri-axis inertial/magnetic sensors package," IEEE Transactions on Neural Systems and Rehabilitation Engineering, vol. 12, no. 2, pp. 295 –302, Jun. 2004.

[28] J. D. Bayliss and D. H. Ballard, "A virtual reality testbed for brain-computer interface research," IEEE Transactions on Rehabilitation Engineering, vol. 8, no. 2, pp. 188 –190, Jun. 2000.

[29] R. E. Kalman, "A New Approach to Linear Filtering and Prediction Problems," Transaction of the ASME-Journal of Basic Engineering, pp. 35-45, March 1960.